Mathematical modeling and analysis of in-situ strength development in cemented paste backfill structure

Liang Cui
Department of Civil Engineering – Lakehead University, Thunder Bay, Ontario, Canada
Mamadou Fall
Department of Civil Engineering – University of Ottawa, Ottawa, Ontario, Canada

ABSTRACT
Cemented paste backfill (CPB) structures are complex underground geomechanical systems. After placement of the fresh CPB into stope (mined-out underground space), a strongly nonlinear and time-dependent variation of material properties and behaviors takes place in CPB mass due the coupled thermo-hydro-mechanical-chemical (THMC) processes. Moreover, the field curing conditions (e.g., CPB-rockmass interaction, stope conditions (geometry, inclination angle, and barricade drainage), and the in-situ temperature) can be significantly different from the laboratory conditions, which may further affect the multiphysics processes and thus the development of CPB strength. Consequently, the actual strength development of CPB in the field may be significantly different from that in the laboratory. Therefore, to accurately and reliably predict the in-situ CPB strength, the effect of the coupled THMC processes must be fully considered and quantitatively assessed. In this study, a coupled multiphysics model for CPB strength is developed and has been successfully validated against the measured data. Then, the validated model is applied to study the changes in the strength of CPB structure under various field conditions (e.g., backfilling strategy, inclination angle of stope, and filling rate). The obtained results provide better insight into the process of the strength increase and spatial distribution in CPB structures as well as contribute to more cost-effective engineering designs of CPB structures.

1 INTRODUCTION

As one of the most novel materials in the backfilling operation of underground stopes (mined-out underground space), cemented paste backfill (CPB, a cementitious material made of tailings, binders, and water) has become a standard practice in underground mines around the world (Cui and Fall 2018a). Due to the financial ramification and severe injuries and/or fatalities induced by the failure of CPB structure(Cui and Fall 2016a), the mechanical stability of CPB structures has been considered as one of the most important design criteria (Cui and Fall 2018b). Therefore, it is of great importance to accurately and reliably assess and predict the mechanical behavior of CPB structure. In this regard, the CPB strength can serve as an adequate indicator of the mechanical stability of CPB structure (Cui 2017). However, after placement into stope, material properties and behaviors of CPB are subjected to complex multiphysics (thermal, hydraulic, mechanical, and chemical) loads (Fall et al. 2015), and field conditions (rock/CPB interface interaction, stope conditions (geometry, inclination angle, barricade drainage conditions), and surrounding rock conditions (e.g., temperature)) (Cui and Fall 2017b). Consequently, accurate prediction of CPB strength is one of the most difficult aspects of CPB design.

To be more specific, Figure 1 can be used to elucidate the coupled thermo-hydro-mechanical-chemcial (THMC) processes that occur in the CPB mass. For the chemical process, the chemical bonds resulted from binder hydration can progressively improve the CPB strength at the macroscopic scale (Jiang et al. 2017). Moreover, for the hydraulic process, the pore water loss due to the binder hydration (liquid pore water to solid phase), and water drainage through barricade structure (a retaining wall structure to keep the CPB within stope) can cause the build-up of suction in the pore space of CPB (Cui and Fall 2017a), and thus contribute to the increase of effective stress which can further enhance CPB strength. For the thermal process, due to the temperature dependence of binder hydration (Cui and Fall 2016b), the thermal process can affect the progress of the chemical reaction in CPB and thus the development of bond strength. In addition, the deformation of CPB induced by the consolidation process control the porosity (or void ratio) dependent material properties (e.g., coefficient of permeability) (Walske 2014). Correspondingly, the mechanical process can affect the development of CPB strength as well. Consequently, the resultant CPB strength can demonstrate strongly nonlinear and time-dependent variation.

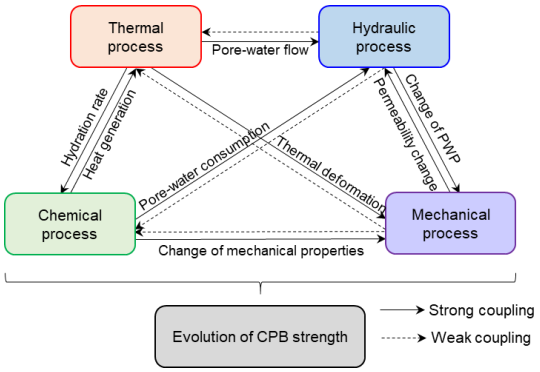

Figure 1. Controlling mechanism responsible for the evolution of CPB strength

Therefore, to accurately predict the development of CPB strength under complex multiphysics loads,

mathematical modeling offers a more effective and attractive alternative compared with experimental investigations. In this paper, a multiphysics model for CPB strength development is presented. The proposed model is validated against measured data, and applied to predict the nonlinear and transient changes of strength in CPB under various field conditions.

2 MATHEMATICAL FORMULATION OF MULTIPHYSICAL MODEL OF CPB STRENGTH

Based on previous studies on CPB strength, the CPB can demonstrate both strain hardening/softening behaviors. Correspondingly, the peak stress from stress-strain curve of unconfined compressive strength (UCS) tests can be used to evaluate the CPB strength. The stress variation with respect to the development of strain can be captured by the evolution of yield surface in the stress space. The following evolutive yield surface proposed by Cui and Fall (2016a) is adopted to reproduce the evolution of yield surface under the effect of binder hydration and the accumulation of plastic strain in CPB.

$$F = \sqrt{J_2} + \alpha(\xi,\kappa)\left[I_1 - C(\xi)\right] = 0 \quad [1]$$

with

$$\begin{aligned}\alpha(\xi,\kappa) &= \frac{2\sin\phi_B(\xi)}{\sqrt{3}\left[3+\sin\phi_B(\xi)\right]} \\ &\quad + B_1\left\{\left[1-\exp(-B_2\kappa)\right] + \left[B_3\kappa\exp(-B_4\kappa)\right]\right\} \\ C(\xi) &= 3c_B(\xi)\cdot\cot\phi_B(\xi)\end{aligned} \quad [2]$$

where α and C represent the material properties of the yield function, and change with degree of binder hydration ξ and effective plastic strain κ ($\kappa = \int\sqrt{2/3 d\varepsilon_p d\varepsilon_p}$ with plastic strain ε_p), B_i is a material parameter and changes with the degree of binder hydration (i=1-4), c_B and φ_B the cohesion and internal friction angle of the CPB, which changes with binder hydration ($c_B = c_B(\xi)$ and $\varphi_B = \varphi_B(\xi)$). The degree of binder hydration (i.e., the extent of chemical reaction) can be evaluated by the following exponential model proposed by Schindler and Folliard (2003).

$$\begin{aligned}\xi\left(w/c, X_{FA}, X_{slag}, T, t\right) = &\left(\frac{1.031\cdot w/c}{0.194 + w/c} + 0.5\cdot X_{FA} + 0.30\cdot X_{slag}\right)\times \\ &\exp\left\{-\left\{\tau\Big/\int_0^t \exp\left[\frac{E_a}{R}\left(\frac{1}{T_r}-\frac{1}{T}\right)\right]dt\right\}^{\beta}\right\}\end{aligned} \quad [3]$$

With

$$\tau = 66.78 x_{C_3A}^{-0.154}\cdot x_{C_3S}^{-0.401}\cdot x_{SO_3}\cdot S_{Blaine}^{-0.804}\cdot\exp\left(2.178X_{slag} + 9.5X_{FA}X_{FA-CaO}\right)$$

$$\beta = 181.4 x_{C_3A}^{0.146}\cdot x_{C_3S}^{0.227}\cdot x_{SO_3}^{0.558}\cdot S_{Blaine}^{-0.535}\cdot\exp\left(-0.647X_{slag}\right)$$

$$E_a(T) = \begin{cases} 33{,}500 + 1{,}470\times(293.15 - T) & T < 293.15K \\ 33{,}500 & T \geq 293.15K \end{cases}$$

Based on the hydration model (Eq.[3]), the effect of binder hydration on the material properties including cohesion (ξ) and internal friction angle φ_B (ξ) can be defined as follows:

$$c_B(\xi) = \exp\left(M_{s1}S_T\right)\cdot\left(1-S_W\right)^{M_{s2}\exp\left(M_{s3}\xi\right)}\cdot M_{c1}\cdot C_m\cdot\xi^{M_{c2}} \quad [4]$$

$$\phi_B(\xi) = \left[\exp\left(N_0 S_T\right)\right]\cdot\left(N_1\xi^{N_2} + N_3\xi\right) \quad [5]$$

where M_{si}, M_{cj}, and N_k are fitting constants (i=1 to 3, j=1 to 2, and k=0 to 3). M_{s1} =-9.6, M_{s2} =724.3, M_{s3}=-4.553, M_{c1}=9507 kPa, M_{c2}=3.2, N_0 =-0.33, N_1 =-176.9°, N_2 =2 and N_3=174.2° are adopted in this study. S_T represents the sulfide mass content with respect to the total mass of dry tailings, S_W refers to the sulfate content in the mixing water; and C_m is the cement content with respect to the total solid mass. Since degree of binder hydration, and sulfide content are incorporated into the material properties of CPB, the effect of mixture receipt can be captured by the proposed model.

The stress invariants I_1 and J_2 can be defined by Biot's effective stress $\boldsymbol{\sigma}'$.

$$\boldsymbol{\sigma}' = \boldsymbol{\sigma} + \left(1 - K_b/K_s\right)\cdot\left(SP_w + \left(1-S\right)P_a\right)\boldsymbol{\delta}_{ij} \quad [6]$$

where $\boldsymbol{\sigma}$ is the total stress tensor, K_b and K_s respectively represent the bulk modulus of the CPB skeleton and solid phase, S is the degree of saturation, P_w and P_a refer to the pore-water and pore-air pressures, and $\boldsymbol{\delta}_{ij}$ is the Kronecker's delta.

Through definition of effective stress (Eq. [5]), the "true" strength of CPB $\boldsymbol{\sigma}_s'$ can be determined.

$$\boldsymbol{\sigma}_s' = \boldsymbol{\sigma}_{axial} + \left(1 - K_b/K_s\right)\cdot\left(SP_w + \left(1-S\right)P_a\right)\boldsymbol{\delta}_{ij} \quad [7]$$

where $\boldsymbol{\sigma}_{axial}$ represent the axial total stress acting on CPB.

With the aid of Eq. (4), the stress invariants I and J_2 can be expressed in terms of $\boldsymbol{\sigma}_{axial}$, and then $\boldsymbol{\sigma}_{axial}$ can be derived through yield function (Eq.[1]) as:

$$\boldsymbol{\sigma}_{axial} = \sqrt{3}C(\xi)\Big/\left[\sqrt{3} - \frac{1}{\alpha(\xi,\kappa_s)}\right] \quad [8]$$

where κ_s denotes the effective plastic strain corresponding to the peak value of $\alpha(\xi, \kappa_s)$, and can be determined through the first derivative test (i.e., $\frac{\partial\alpha(\xi,\kappa)}{\partial\kappa}$=0) of $\alpha(\xi, \kappa)$,with respect to the effective plastic strain κ.

$$\kappa_s = \frac{B_2^2 + B_4 + \sqrt{B_4^2 + B_2^2 B_4 - B_2^4}}{B_2^3} \quad [9]$$

with

$$B_1 = R_{\alpha 1}\xi^{R_{\alpha 2}} + R_{\alpha 3}$$
$$B_2 = R_{\alpha 4}\xi^{R_{\alpha 5}} + R_{\alpha 6} \quad [10]$$
$$B_3 = R_{\alpha 7}\xi^{R_{\alpha 8}} + R_{\alpha 9}$$
$$B_4 = R_{\alpha 10}\xi^{R_{\alpha 11}} + R_{\alpha 12}$$

where $R_{\alpha i}$ is a fitting constant (i=1 to 12) and depends on the type of CPB. $R_{\alpha 1}$=-0.05, $R_{\alpha 2}$=4.178, $R_{\alpha 3}$=0.071, $R_{\alpha 4}$=-200, $R_{\alpha 5}$=10, $R_{\alpha 6}$=360.5, $R_{\alpha 7}$=832.3, $R_{\alpha 8}$=3, $R_{\alpha 9}$=110, $R_{\alpha 10}$=260.1, $R_{\alpha 11}$=3.5 and $R_{\alpha 12}$=80, as suggested by Cui and Fall (2016a) are adopted in this study.

Then, the axial total stress $\boldsymbol{\sigma_{axial}}$, and the true strength $\boldsymbol{\sigma'_s}$ of CPB can be derived by substituting Eqs. [7], [6], and [2] into Eq. [1]:

$$\sigma_{axial} = \frac{3\sqrt{3}c_B(\xi)\cdot\cot\phi_B(\xi)}{\sqrt{3}+1\Big/\left\{\frac{2\sin\phi_B(\xi)}{\sqrt{3}\left[3+\sin\phi_B(\xi)\right]}+B_1\left\{\left[1-\exp(-B_2\kappa_s)\right]+B_3\kappa_s\exp(-B_4\kappa_s)\right\}\right\}} \quad [11]$$

$$\sigma_s = \left(1-K_b\Big/K_s\right)\left[SP_w+(1-S)P_a\right]\delta_{ij} +$$

$$\frac{3\sqrt{3}c_B(\xi)\cdot\cot\phi_B(\xi)}{\sqrt{3}+1\Big/\left\{\frac{2\sin\phi_B(\xi)}{\sqrt{3}\left[3+\sin\phi_B(\xi)\right]}+B_1\left\{\left[1-\exp(-B_2\kappa_s)\right]+B_3\kappa_s\exp(-B_4\kappa_s)\right\}\right\}} \quad [12]$$

with

$$\kappa_s = \frac{B_2^2+B_4+\sqrt{B_4^2+B_2^2B_4-B_2^4}}{B_2^3}$$

As shown in Eq. [9], the prediction of true strength of CPB requires the evaluation of pore water pressure and degree of saturation. However, as discussed in the Section, Introduction, the behaviors and performance of CPB mass are controlled by the coupled THMC process. Therefore, to capture the hydraulic process in CPB, the analytical description of coupled Multiphysics is needed. In this regard, the fully coupled THMC model developed by Cui and Fall (2015a) is adopted in this study. In this model, the conservation principles of mass (pore water and pore air), momentum (solid phase), and energy (heat transfer and generation) were used to capture the interaction of multiphysics and their effect on the material properties and behaviors of CPB mass.

$$\phi S\frac{\partial\rho_w}{\partial t}+\phi\rho_w\frac{\partial S}{\partial t}+S\rho_w\left[\frac{\partial\varepsilon_v}{\partial t}+\frac{(1-\phi)}{\rho_s}\frac{\partial\rho_s}{\partial t}\right]-\nabla\cdot\left(\phi S\rho_w k\frac{k_{rw}}{\mu_w}\nabla\left(P_w-\rho_w g\right)\right)$$
$$=\phi S\left(\frac{\rho_w}{\rho_s}S-1\right)\left\{2m_{hc0}\left(0.187x_{C_3S}+0.158x_{C_2S}+0.665x_{C_3A}+0.2130x_{C_4AF}\right)\right.$$
$$\left.\times\left\{\left(\frac{\tau}{t_e}\right)^{\beta}\left(\frac{\beta}{t_e}\right)\xi\exp\left[\frac{E_a}{R}\left(\frac{1}{273+T_r}-\frac{1}{273+T}\right)\right]\right\}\right. \quad [13]$$

$$\phi(1-S)\frac{\partial\rho_a}{\partial t}-\phi\rho_a\frac{\partial S}{\partial t}+(1-S)\rho_a\left[\frac{(1-\phi)}{\rho_s}\frac{\partial\rho_s}{\partial t}+\frac{\partial\varepsilon_v}{\partial t}\right]=\left[(1-S)\phi S\rho_a\Big/\rho_s\right]$$
$$+\nabla\cdot\phi(1-S)\rho_a k\frac{k_{ra}}{\mu_a}\nabla\left(P_a-\rho_a g\right)\left\{2m_{hc0}\left(0.187x_{C_3S}+0.158x_{C_2S}+0.665x_{C_3A}+0.2130x_{C_4AF}\right)\right\} \quad [14]$$
$$\times\left\{\left(\frac{\tau}{t_e}\right)^{\beta}\left(\frac{\beta}{t_e}\right)\xi\exp\left[\frac{E_a}{R}\left(\frac{1}{273+T_r}-\frac{1}{273+T}\right)\right]\right\}$$

$$\nabla\cdot\left(\frac{\partial\boldsymbol{\sigma}}{\partial t}\right)+\frac{\partial\left[(1-\phi)\rho_s+\phi S\rho_w+\phi(1-S)\rho_a\right]}{\partial t}\boldsymbol{g}=0 \quad [15]$$

$$\left[\left(\frac{1}{1+e}\right)\rho_s C_s+\frac{e}{1+e}S\rho_w C_w+\frac{e}{1+e}(1-S)\rho_a C_a\right]\frac{\partial T}{\partial t}+\nabla\cdot\left(-k_{eff}\nabla T\right)$$
$$+\left(\rho_w C_w\mathbf{v}^{rw}+\rho_a C_a\mathbf{v}^{ra}\right)\cdot\nabla T=\left(H_c\cdot X_c+461\cdot X_{slag}+1800\cdot x_{CaO/FA}\cdot X_{FA}\right) \quad [16]$$
$$\times C_b\left(\frac{\tau}{t_e}\right)^{\beta}\cdot\left(\frac{\beta}{t_e}\right)\cdot\xi\cdot\exp\left[\frac{E_a}{R}\left(\frac{1}{273+T_r}-\frac{1}{273+T}\right)\right]$$

where ρ_i is the density (i=air, water and solid), ε_v is the volumetric strain, k is the intrinsic permeability of CPB, k_{ri} represents the relative permeability, μ_i refer to the dynamic viscosity, C_i is the specific heat capacity, v^{ri} is Darcy's velocity, g is the gravitational acceleration, m_{hc0} is the initial cement mass, k_{eff} is the effective thermal conductivity, H_c is the total heat released by hydration, C_b is the apparent binder density relative to the total volume of the CTB mixture. The detailed information on the constitutive relations and predictive functions of material properties for the fully coupled THMC model are provided in (Cui and Fall 2015a, b).

3 MODEL VALIDATION AGAINST EXPERIMENTAL DATA

To validate the predictability of the developed multiphysics strength model, a laboratory monitoring and testing program was conducted in this study. To integrate the effect of initial temperature into the development of CPB strength, three different initial temperature of 5°C, 25°C, and 35°C were adopted for the preparation of CPB samples. For the mixture recipe for preparing CPB samples, PC type I with cement content (wt%) of 4.5%, and ground silica tailings were mixed with tap water (water to cement ratio of 7.6). The fresh CPB was placed into a cylindrical mold (100mm diameter × 200mm height). Moreover, the suction and temperature sensors were installed in the sample to continuously measure the change of pore water pressure and temperature in CPB. The sample mold was covered by a thermal insulation material to imitate the slow rate of heat transfer between CPB and rock mass in a stope. Then, the CPB samples with different curing times (1, 3 and 7 days) were employed to investigate the development of strength.

The multiphysics strength model was implemented into Comsol Multiphysics to predict the change of CPB strength under the specified curing conditions in this monitoring program. The adopted initial and boundary conditions are tabulated in Table 1. The axisymmetric geometry model was used to simulate the cylindrical CPB sample (see Figure 2).

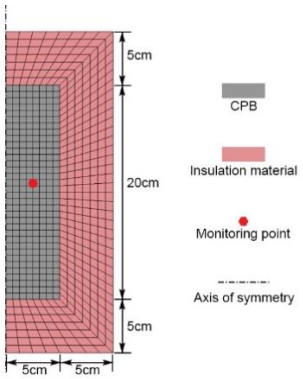

Figure 2. Mesh and geometry of simulated cell test.

Table 1. Initial values and boundary conditions for the model validation

Parameter	Value
Initial temperature (°C)	5, 25 and 35
Surrounding temperature (°C)	22
Initial hydraulic head	0
Body force (m/s^2)	9.81
Hydraulic B.C.	No flow (surrounding surface)
Mechanical B.C.	Free (top surface) Roller (later side) Fixed (bottom side)

*B.C.: boundary condition

The measured data and predicted results of pore water pressure (PWP) and temperature are shown in Figure 3 and 4, respectively. As shown in these figures, the initial temperature can significantly affect the change of PWP and temperature. Specifically, the warmer initial temperature can accelerate the binder hydration and thus increase the pore water consumption for a given period of curing time. As a result, the pore water becomes more negative in CPB sample under warmer temperature (re: Figure 3). However, the effect of initial temperature on the evolution of temperature in CPB sample mainly takes place in the very early age, and then the temperature of all samples gradually approaches the room temperature (22°C). From Figure 3 and 4, the good agreement between measured and predicted results can confirm that the developed model can accurately capture the evolution of PWP (hydraulic process) and temperature (thermal process). Moreover, as discussed in the Section, Introduction, the change of PWP and temperature are controlled by the coupled THMC. Therefore, the excellent agreement between simulation results and measured data also indicate the prediction capacity of the model for the coupled multiphysics process in CPB.

For the development of CPB strength, the measured data from UCS test in accordance with ASTM C39 were depicted in Figure 5. Based on the obtained results, it can be found that (1) with the advance of binder hydration (i.e., the elapse of curing time), the CPB strength can be improved significantly. Taking the CPB sample with an initial temperature of 25°C as an example, the UCS value increases from 128 kPa (1-day CPB sample) to 356 kPa (7-day CPB sample) (increase by 178%). The considerable improvement of CPB strength can fully demonstrate the significant contribution of binder hydration; (2) The initial temperature can affect the development of CPB strength, especially for the early-age CPB samples. For example, compared with UCS value (65 kPa) of 1-day CPB sample with an initial temperature of 5°C, an apparent strength improvement of CPB strength (165 kPa, increase by 154%) was observed in the counterpart sample with an initial temperature of 35°C. The obtained result can indicate that the initial temperature (i.e., the thermal process) can have significant impacts on the development of CPB strength. Through the comparison between the simulation results and measured data, a good agreement is obtained in terms of both evolutionary trend and magnitude. Therefore, the developed model can be used to predict the development of CPB strength under the effect of the coupled THMC processes.

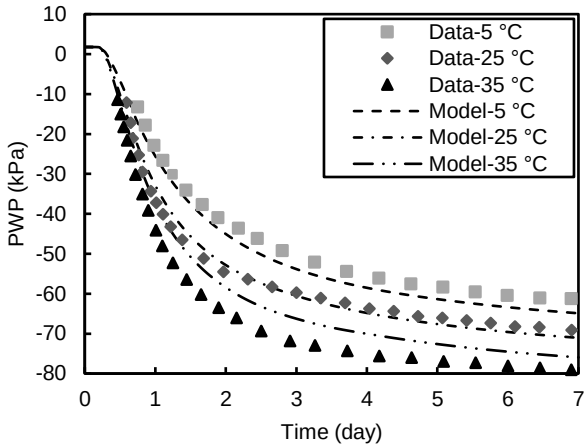

Figure 3. Comparison of predicted results and experimental values of pore water pressure (PWP).

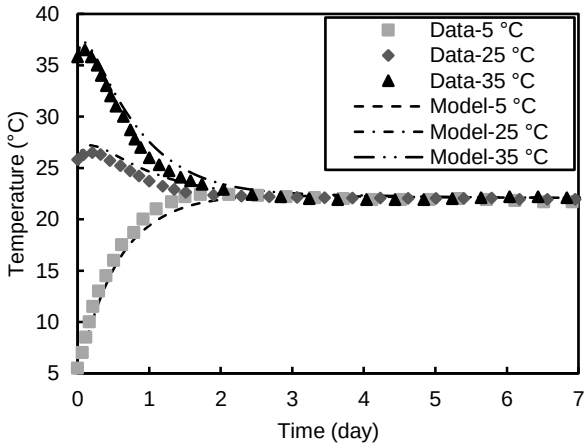

Figure 4. Comparison of predicted results and experimental values of temperature.

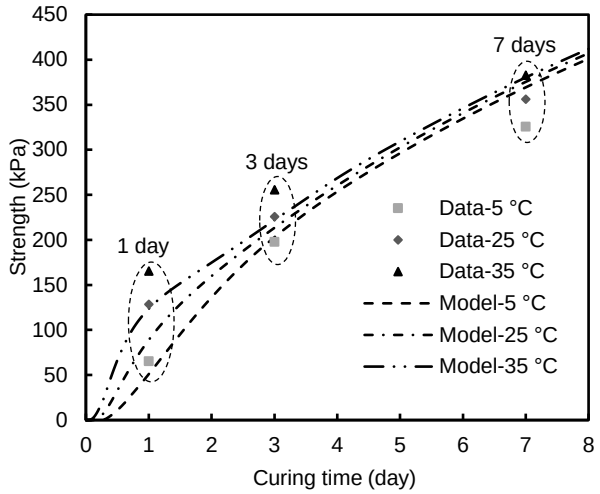

Figure 5. Comparison of predicted results and experimental values of true CTB strength.

4 MODEL APPLICATION

The validated multiphysics model was used to numerically investigate the changes in CPB strength in the stope under various field conditions including stope geometry, and inclination angle, and filling rates. To clearly demonstrate the changes of CPB strength under various field condition, a control stope with dimensions of 8 m (W)×16 m (H) was adopted as a reference (see Figure 6). The barricade structure has a dimension of 4 m (W)×4 m (H).

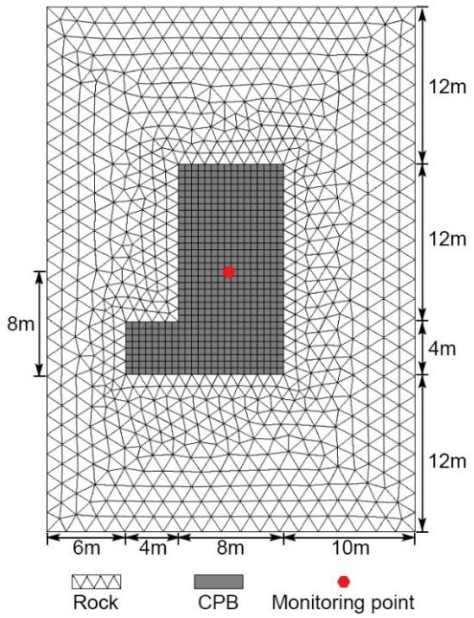

Figure 6. Mesh and geometry of control stope.

The boundary conditions and initial values adopted by the control stope are listed in Table 2. All numerical investigations were carried out through the specified modification of the control stope.

Table 2. Initial values and boundary conditions for control stope

Parameter	Value
Mixture recipe	
Cement content (wt%)	Residual fill: 4.5, and plug fill: 7
w/c ratio	7.6
Initial void ratio	1
Filling rate (m/h)	0.5
Filling strategy	2-stages with 1-day plug
Surrounding rock mass	
Density (kg/m3)	2500
Young's modulus (GPa)	30
Poisson's ratio	0.3
Thermal conductivity (W/m K)	3.9
Heat capacity (J/Kg K)	790
Mechanical component	
Top surface	Free
Lateral sides	Roller
Bottom side	Fixed
Body force	Gravity
Hydraulic component	
Surrounding sides	No flow
Body force	Gravity
Initial value	Hydraulic head=0
Thermal component	
Surrounding surfaces (°C)	25
Initial temp. (°C)	25

4.1 Effect of Stope Geometry

Different stoping methods and mining plans may result in various stope geometries. Therefore, it is necessary to investigate the effect of stope geometry on the development of CPB strength. In this study, three different stopes (5 m (W)×10 m (H), 8 m (W)×16 m (H), and 10 m (W)×20 m (H)) were considered. The spatial distribution of CPB strength with different curing times is shown in Figure 7. From this figure, it can be found that stope geometry can affect the development of CPB strength. The CPB strength in larger stope is higher than that obtained in small stope. This is because due to the binder hydration, more heat can be generated in the larger stope. As a result, the binder hydration can advance to a larger extent in larger stope, and thus further contribute to the improvement of CPB strength. The obtained results are consistent with the experimental investigation conducted in this study (see Figure 5) and the previous study (Nasir and Fall 2010). Moreover, based on the simulation result, it can be observed that the non-uniform distribution becomes more apparent with curing time. This is mainly attributed to (1) PWP changes due to the self-desiccation process and water drainage through the barricade, and (2) the inconsistent initial temperatures between CPB mass and rock mass. As a result, the mass (pore water) and heat transfer contributes to the non-uniformly spatial distribution of CPB strength. Therefore, this case study not only confirms the effect of stope geometry on CPB strength but indicates the necessity of incorporation of fully coupled THMC process into the prediction of CPB strength.

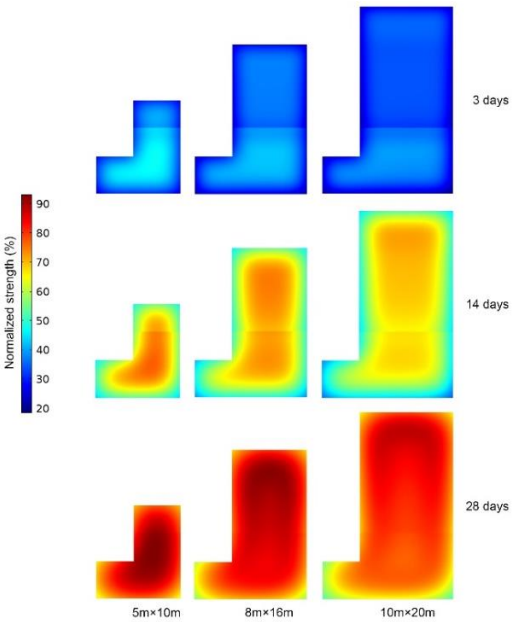

Figure 7. Effect of stope geometry on the evolution of CPB strength.

4.2 Effect of Inclination Angle of Stope

Apart from stope geometry, the natural existence of orebodies can also cause various inclination angles. Hence, the optimal design of CPB structure necessitates the investigation of the effect of inclination angle on the development of CPB strength in the stope. In this study, three different cases were considered (stope with an inclination angle of 90°, 70° and 50°). The comparison of the CPB strength in the stopes with different inclination angles is shown in Figure 8. It can be observed that the change of inclination angle causes very limited changes of CPB strength magnitude. However, the large inclination angle can further contribute to the non-uniformly spatial distribution of CPB strength. For the investigated stopes with same filling height (8 m), the inclined stope will accommodate more CPB mass. Correspondingly, the hanging wall and foot wall have larger dimensions for the inclined stopes, which can further contribute to the heat transfer between the surrounding rock and CPB. As a result, the spatial distribution of CPB strength becomes more non-uniform in the inclined stope.

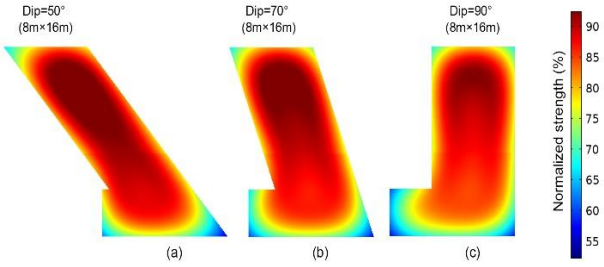

Figure 8. Effect of inclination angle on the spatial distribution of strength of CPB with curing time of 28-days.

4.3 Effect of Filling Rate

Due to the differences in mining operation, the adopted filling rate may be different from one stope to another. The filling rate affects the curing time of CPB material and thus its strength development. In addition, the filling rate directly affects the mining cycles and productivity. Due to the significance of filling rate, the investigation of the effect of filling rate on the CPB strength was conducted in this study. To study the effect of filling rate, three different filling rates including 1 m/h, 0.5m/h, and 0.25 m/h were adopted. To demonstrate the change of CPB strength, the predicted values at the monitoring point were plotted in Figure 9. It can be seen that higher strength is formed in CPB with a lower filling rate after the rest period of plug layer. This is because lower filling rate can yield longer curing time for a given filling height, and thus contribute to the improvement of CPB strength. Therefore, the developed model can capture the effect of filling rate on the changes of CPB strength.

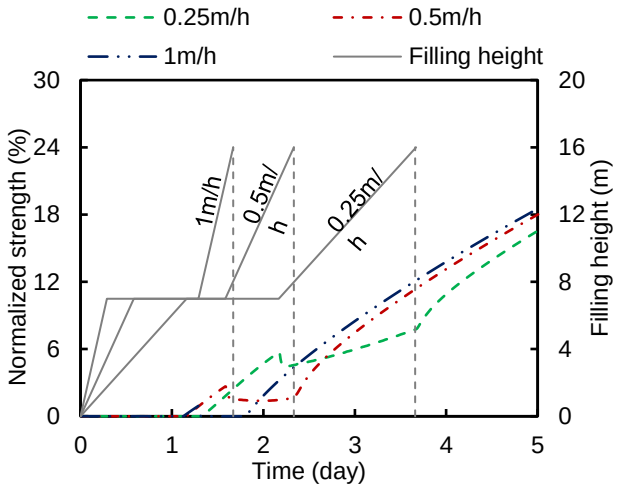

Figure 9. Effect of filling rate on changes to CTB strength.

5 CONCLUSIONS

An integrated multiphysics model on CPB strength is developed to predict the development of CPB strength under the influence of coupled THMC processes. The predictability of the proposed model is validated against the experimental data. The validation results indicate the developed model can accurately capture the change of Multiphysics process and the CPB strength under different curing conditions. Based on the obtained results of model application, it has been found that the stope conditions (i.e., stope geometry and inclination angle) can significantly affect the development and spatial distribution of CPB strength. In addition, the inclination angle can further contribute to the non-uninformly spatial distribution of CPB strength. The obtained results indicate that the accurate and reliable assessment and prediction of in-situ CPB strength requires the full consideration of coupled THMC processes. Therefore, the developed Multiphysics model on CPB strength can be used an effective tool for the optimal design of CPB structure.

6 REFERENCES

Cui, L. 2017. Multiphysics Modeling and Simulation of the Behavior of Cemented Tailings Backfill. University of Ottawa, Canada.

Cui, L., and Fall, M. 2015a. A coupled thermo-hydro-mechano-chemical model for underground cemented tailings backfill. Tunn Undergr Sp Tech **50**: 396-414.

Cui, L., and Fall, M. 2015b. Multiphysics Modelling of the Behaviour of Cemented Tailings Backfill Materials. *In* International Conference on Civil, Structural and Transportation Engineering. Internatioanl ASET Inc., Ottawa, ON, Canada. pp. 1-7.

Cui, L., and Fall, M. 2016a. An evolutive elasto-plastic model for cemented paste backfill. Comput Geotech **71**: 19-29.

Cui, L., and Fall, M. 2016b. Mechanical and thermal properties of cemented tailings materials at early ages: Influence of initial temperature, curing stress and drainage conditions. Constr Build Mater **125**: 553-563.

Cui, L., and Fall, M. 2017a. Modeling of pressure on retaining structures for underground fill mass. Tunn Undergr Sp Tech **69**: 94-107.

Cui, L., and Fall, M. 2017b. Multiphysics modeling of arching effects in fill mass. Comput Geotech **83**: 114-131.

Cui, L., and Fall, M. 2018a. Mathematical modelling of cemented tailings backfill: a review. Int J Min Reclam Environ: 1-20.

Cui, L., and Fall, M. 2018b. Multiphysics Modeling and Simulation of Strength Development and Distribution in Cemented Tailings Backfill Structures. International Journal of Concrete Structures and Materials **12**(1): 25.

Fall, M., Nasir, O., Cui, L., and Han, F. 2015. Coupled modeling of the strength development and distribution within cemented paste backfill structure. *In* 49th US Rock Mechanics/Geomechanics Symposium. American Rock Mechanics Association, San Francisco, California, USA. pp. 587-595.

Jiang, H., Fall, M., and Cui, L. 2017. Freezing behaviour of cemented paste backfill material in column experiments. Constr Build Mater **147**: 837-846.

Nasir, O., and Fall, M. 2010. Coupling binder hydration, temperature and compressive strength development of underground cemented paste backfill at early ages. Tunn Undergr Sp Tech **25**(1): 9-20.

Schindler, A.K., and Folliard, K.J. 2003. Influence of supplementary cementing materials on the heat of hydration of concrete. *In* Advances in Cement and Concrete IX Conference. Engineering Conferences International, Inc., Colorado, USA. pp. 17-26.

Walske, M.L. 2014. An experimental study of cementing paste backfill. University of Western Australia, Perth, Australia.